

# Effects of Temperature Variations on Precast, Prestressed Concrete Bridge Girders

P. J. Barr, M.ASCE<sup>1</sup>; J. F. Stanton, M.ASCE<sup>2</sup>; and M. O. Eberhard, M.ASCE<sup>3</sup>

**Abstract:** The monitoring of a precast, prestressed girder bridge during fabrication and service provided the opportunity to observe temperature variations and to evaluate the accuracy of calculated strains and cambers. The use of high curing temperatures during fabrication affects the level of prestress because the strand length is fixed during the heating, the coefficients of thermal expansion of steel and concrete differ, and the concrete temperature distribution may not be uniform. For the girders discussed here, these effects combined to reduce the calculated prestressing stress from the original design values at release by 3 to 7%, to reduce the initial camber by 26 to 40%, and to increase the bottom tension stress in service by 12 to 27%. The main effect of applying the standard service temperature profiles to the bridge was to increase the bottom stress by 60% of the allowable tension stress. These effects can be compensated for by increasing the amount of prestressing steel, but in highly stressed girders, such an increase leads to increased prestress losses (requiring yet more strands) and higher concrete strength requirements at release.

**DOI:** 10.1061/(ASCE)1084-0702(2005)10:2(186)

**CE Database subject headings:** Temperature effects; Concrete, prestressed; Concrete, precast; Bridges, concrete; Bridges, girder; Monitoring.

## Introduction

Numerous approaches have been proposed to extend the practical span range of precast, prestressed bridge girders. For example, Seguirant (1998) developed deeper precast cross sections that can be pretensioned during fabrication and post tensioned on site. Span-to-span, live-load girder continuity has been used to reduce peak live-load moments (Ma et al. 1998). The development of high-performance concrete also makes possible the use of longer spans, mainly by increasing the level of prestressing that can be applied to a girder (Burns et al. 1997; Barr et al. 2000a).

Improvements in modeling accuracy, which make it possible to reduce factors of safety, can further lengthen the practical span range of girders. For example, the current load and resistance-factored design specifications for bridges (AASHTO 1998) provide equations to calculate live-load distribution factors that are generally less conservative than equations specified previously (AASHTO 1996; Barr et al. 2001). Similarly, the use of complex time-stepping models of prestress loss usually leads to lower loss estimates and consequently longer span capabilities (Lwin and Khaleghi 1997).

In spite of all these developments, the basis for girder design

has changed little over the past 30 years. Prestressed concrete members must satisfy working-stress requirements under service loads and strength requirements under factored loads (AASHTO 1998; ACI 1999). Working stress limits for flexure usually control the selection of cross section and prestressing steel. In particular, the design of precast, prestressed concrete bridge girders is usually controlled by the flexural stress in the bottom flange,  $f_{bot}$ . This stress is computed from elastic beam theory as follows:

$$f_{bot} = -\frac{P_i}{A} \left( 1 + \frac{ec_{bot}}{r^2} \right) + \frac{M_{DL}}{S_g} \quad (1a)$$

under initial conditions and

$$f_{bot} = -\frac{P_e}{A} \left( 1 + \frac{ec_{bot}}{r^2} \right) + \frac{M_{DL}}{S_g} + \frac{M_{SIDL}}{S_{comp}} + \frac{M_{LL}}{S_{comp}} \quad (1b)$$

under effective, or service, conditions. This stress must satisfy

$$f_{bot} \geq f_{ci,all} \quad (1c)$$

and

$$f_{bot} \leq f_{te,all} \quad (\text{tension is positive}) \quad (1d)$$

where  $P_e$  = effective prestress force (after accounting for prestress losses);  $A$  = girder cross-sectional area;  $e$  = distance from centroid of girder to centroid of prestressing force;  $c_{bot}$  = distance from centroid of girder to bottom of girder;  $r$  = girder cross-section radius of gyration =  $\sqrt{I/A}$ ;  $M_{DL}$  = moment due to weight of girder and deck;  $M_{SIDL}$  = superimposed dead-load moment (e.g., barriers and diaphragms);  $M_{LL}$  = moment due to live-load;  $f_{ci,all}$ ,  $f_{te,all}$  = allowable stresses in compression and tension under initial and effective conditions respectively; and  $S_g$ ,  $S_{comp}$  = section modulus of bare girder and composite section. At release, Eq. (1c) places an upper bound on the level of prestressing steel. In service, Eq. (1d) limits the magnitude of the allowable live load.

These calculations account for many sources of stress, including the effects of applied loads ( $M_{DL}$ ,  $M_{SIDL}$ ,  $M_{LL}$ ) and of pre-

<sup>1</sup>Assistant Professor, Dept. of Civil and Environmental Engineering, Utah State Univ., Box 4110, Logan, UT 84322.

<sup>2</sup>Professor, Dept. of Civil and Environmental Engineering, Univ. of Washington, Box 352700, Seattle, WA 98195.

<sup>3</sup>Associate Professor, Dept. of Civil and Environmental Engineering, Univ. of Washington, Box 352700, Seattle, WA 98195.

Note. Discussion open until August 1, 2005. Separate discussions must be submitted for individual papers. To extend the closing date by one month, a written request must be filed with the ASCE Managing Editor. The manuscript for this paper was submitted for review and possible publication on September 4, 2002; approved on January 5, 2004. This paper is part of the *Journal of Bridge Engineering*, Vol. 10, No. 2, March 1, 2005. ©ASCE, ISSN 1084-0702/2005/2-186-194/\$25.00.

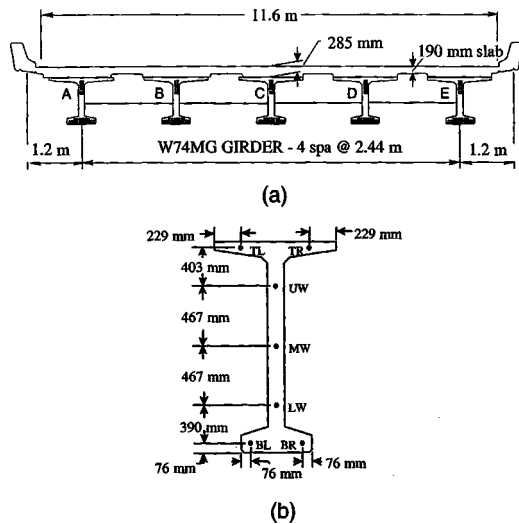


**Fig. 1.** SR18/SR516 Bridge: (a) Cross section; and (b) layout of vibrating-wire strain gauges

stress ( $P_c$ ), which in turn includes estimates of losses attributable to steel relaxation and to elastic shortening, shrinkage, and creep of the concrete. By contrast, the specification does not require the effects of temperature variations to be included, so they are commonly ignored, even though they can be significant [e.g., Imbsen et al. (1985)]. This omission may stem from a belief that these effects are small, or perhaps from the paucity of guidance available to account for temperature effects, particularly those attributable to fabrication conditions. The effects of temperature variation on girder performance need to be understood better.

This paper summarizes observations, during both fabrication and service, of temperature variations and their effects (e.g., changes in stresses, strains, and cambers) for a typical precast, prestressed concrete girder bridge. Based on these observations and on the simple theory presented in the appendix, tools are developed to gauge the effects of temperature variations. The significance of these variations for design is quantified in terms of changes in the required concrete strength at release of prestress and changes in the required amount of prestressing steel.

## Experimental Program

To collect data on the behavior of a typical precast girder bridge, a new three-span bridge [Fig. 1(a)] was instrumented during fabrication and monitored for 3 years (Barr et al. 2000a). This bridge, which carries Washington State Route 18 over State Route 516 (SR18/SR516 bridge), has span lengths of 24.4, 41.7, and 24.4 m (80, 137, and 80 ft). The cast-in-place roadway deck is 190-mm (7.5-in.) thick, has a width of 11.6 m (38 ft), and is supported by five lines of Washington State W74MG girders (girder lines A–E). In addition, a 20-ft long, statically determinate girder, designated the “test girder,” was cast at the same time as the bridge girders and with the same cross section and materials.

Vibrating-wire strain gauges (VWSGs), which monitored changes in temperature and strain, were embedded in both the bridge and test girder. These sensors, with a gauge length of 152 mm (6 in.), were selected for this task because of their history of long-term reliability (Burns et al. 1997). Sets of gauges were embedded at midspan and at 1.52 m (5 ft) from one end in the test girder and in five bridge girders. The layout of the midspan

gauges for the test girder is shown in Fig. 1(b), in which the gauge designations shown refer to top left (TL), top right (TR), upper web (UW), middle web (MW), lower web (LW), bottom left (BL), and bottom right (BR) gauges. In the bridge girders, the gauge layout was identical to that at midspan in the test girder, except that only one gauge was placed in the top flange (TG). For each instrumented girder, the bottom gauges (BL and BR) were placed at the same elevation as the centroid of the prestressing strand.

A stretched-wire system was used to measure changes in camber. Stretched-wire systems have been used by various researchers to measure deflections in structures [e.g., Ghali and Elbadry (1997); Vurpillot et al. (1998)]. In the most common form of this device, a wire is stretched between the two ends of a girder, and an observer manually monitors the relative displacement between the wire and a scale attached to the girder at midspan. In the system developed for this study (Stanton et al. 2003), the relative displacement between the girder and wire was monitored automatically with an LVDT. In addition, a combination of weights and pulleys was used to reduce the errors caused by thermal expansion and live-load vibration. Stanton et al. (2002) provide details of the device and an analysis of its resolution. The stretched-wire device used on the SR18/SR516 Bridge had a theoretical resolution of 1 mm (0.04 in.).

## Response to Temperature Variations

Variations in temperature distribution in bridge members can be described in terms of a uniform component and a temperature gradient; the average (uniform) temperature change only causes changes in axial length of the member, while the temperature gradient causes bending deformations. In structures that are externally statically determinate, such as simple-span bridges, these deformations occur without inducing external forces, and these deformations occur without inducing external forces, and the main design consequence of temperature variations is that these deformations must be accommodated. For example, the designer needs to provide bearings with adequate displacement and rotation capacities. In some skew bridges, longitudinal expansion may cause some lateral displacement (Moorty and Roeder 1992).

In structures that are externally statically indeterminate, forces are induced that restrain these temperature-induced deformations. If longitudinal expansion is prevented, the girder may experience large axial forces, which could lead to damage at the bearings or abutments (Imbsen et al. 1985). If the girders are continuous, bending moments will be induced at the intermediate supports. These bending moments are similar in concept to the secondary moments caused by prestressing.

Indeterminacy also occurs over the cross section and will be referred to here as internal indeterminacy. If the temperature distribution is nonlinear over the height of the girder, thermally induced stresses will develop during curing and in service. By contrast, stresses due to external indeterminacy are unlikely to occur during curing because the members are simply supported at that time.

Both types of indeterminacy (external and internal) contribute to the concrete stress. The relative magnitudes of the contributions depend on the bridge properties and the temperature distribution. A methodology with which to compute the magnitude of stress and camber changes resulting from variations in temperature is derived in the appendix. The following sections describe temperature variations observed in the SR18/SR516 Bridge dur-

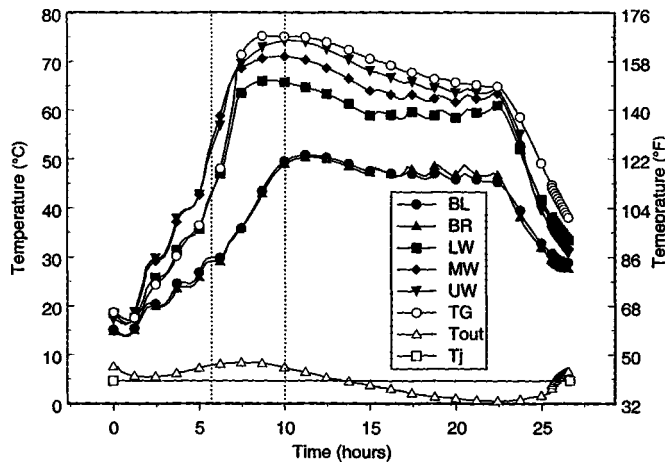


Fig. 2. Concrete temperature history during curing: Girder 2B

ing curing and in service and estimate the effects of these variations.

### Effects of Elevated Curing Temperatures

During curing, precast fabricators usually heat the concrete to reduce the time needed to achieve the specified release strength. This heating affects the concrete properties (Mehta and Monteiro 1993) and can also affect the camber at release (Burns et al. 1997). Some researchers (Acker and Hassan 1978; Huang 1982) have conducted nonlinear thermomechanical analyses to show that the strand stress at release may also be affected. However, designers rarely if ever account for thermal effects during curing. The following discussion addresses the effects of changes in temperature while the concrete is curing. Predictive equations are developed and illustrated using measured values from one of the bridge girders.

### Recorded Temperature Histories

Fig. 2 shows the temperature histories recorded for each gauge embedded at midspan of Girder B in Span 2 (Girder 2B) of the bridge, from casting through destressing. Readings were taken at 2 and 15 min intervals during those two times. After destressing, the girders were transported to the storage yard and so the recordings were temporarily stopped in order to avoid damaging the

equipment, but they were resumed within an hour of destressing. The figure also shows the temperature recorded at the time the strands were prestressed,  $T_j$ , and the ambient outside temperature during curing,  $T_{out}$ . The temperature histories for the test girder and remaining four instrumented bridge girders were similar and are provided in Barr (1998).

In Fig. 2, time 0 corresponds to the time that Girder 2B was cast (7:15 a.m. on March 10, 1997). The ripples in the temperature readings correspond to the activation of the steam curing system. During the first few hours (hours 1 to 6), the temperature in the concrete actually decreased each time the steam curing was shut off. This phenomenon was a result of the cold ambient temperature (approximately 5°C) and the admixtures in the concrete mix that delayed the start of hydration. After about 6 h, hydration of the cement caused the concrete temperature to increase monotonically, even when the steam curing system was inactive. After approximately 22 h, the steam system was deactivated and the curing blanket was removed, which caused the girder to cool rapidly.

Fig. 2 shows that during curing the concrete temperature varied substantially over the height of the girder. The temperature was lowest at the bottom of the girder (gauges BL and BR) and highest at the top (Gauge TG). The peak temperature difference between the top and bottom was more than 30°C (54°F). This difference can be attributed to the girders' being cast outside during winter, so the ground acted as a heat sink and cooled the bottom of the girder. In addition, the forms were heated externally by steam, which rose to the top of the insulated blanket. Of course, the magnitude of other thermal gradients will depend on the outside temperature and the method used to heat the particular girder.

High curing temperatures affect prestress forces and cambers in at least three ways. First, heating the prestressing strand, while its length is fixed between the abutments, leads to prestress loss  $\Delta f_{p1}$  and a resulting change in camber,  $\delta_1$ . Second, if the coefficient of thermal expansion of the concrete exceeds that of the prestressing steel, the prestressing stress decreases ( $\Delta f_{p2}$ ), as does the camber,  $\delta_2$ , when the beam cools. Finally, if the curing temperature distribution has a significant gradient when the concrete hardens, the level of prestressing and camber change further ( $\Delta f_{p3}$  and  $\delta_3$ ). Each of these factors is addressed in turn, and their effects are summarized in Table 1.

Table 1. Calculated Effects of Temperature Variations for Bonding Time of 10 h

Effects	Behavior			Design	
	$f_p$ at release (MPa)	Camber at release (mm)	$f_c$ at service (MPa)	$A_p$ (mm <sup>2</sup> )	$f'_{ci}$ (MPa)
<b>Initial design values without thermal effects of curing</b>	1,240	99	4.1	5,550	51
Curing Effect 1	-81.7	-10.0	1.1	670	2.3
Curing Effect 2	-11.6	7.8	0.2	390	0.3
Curing Effect 3	10.1	-37.8	-0.2	-380	-0.2
Total effect of curing	-83.1	-40.0 <sup>a</sup>	1.1	680	2.4
<b>Effect of service temperature</b>					
Simply supported (Zone 1)	(-)	(-)	0.42 <sup>b</sup>	153	1.6
Continuous (Zone 1)	(-)	(-)	2.5	760	10.7

<sup>a</sup>Measured camber at release was 68 mm.

<sup>b</sup>Neglecting the effect of live load continuity and multiplying the positive temperature gradient by -0.3.

## Effects of Heating Strand before It Bonds to Concrete

During the early stages of curing, the concrete and prestressing strand temperature increases, which leads to the following mechanism of stress loss. The strands are stressed at ambient temperature, but when they are heated they cannot expand (their length is fixed by the abutments), so the strand stress reduces. The magnitude of stress loss is fixed and irrecoverable once the strand bonds to the concrete.

To estimate the magnitude of this stress loss, consider a prestressed member that is cured by placing a blanket over a portion of the casting bed and applying external heat underneath the blanket. The member occupies some but not all of the blanket length. The temperature at the time of initial strand jacking is  $T_j$ . Until the concrete bonds to the strands, the change in strand stress can be calculated based on the strand temperatures in the girder ( $T_g$ ), in the bare strand inside the thermal blanket ( $T_{in}$ ), and in the strand outside the blanket ( $T_{out}$ ). This change in strand stress before bonding,  $\Delta f_{p1}$ , is

$$\Delta f_{p1} = -\frac{\alpha_p E_p}{L_{bed}} \{ (T_{out} - T_j) L_{out} + (T_{in} - T_j) L_{in} + (T_g - T_j) L_g \} \quad (2)$$

where  $\alpha_p$  = coefficient of thermal expansion of prestressing strand;  $E_p$  = modulus of elasticity of prestressing strand;  $L_{out}$ ,  $T_{out}$  = length and temperature of strand outside blanket (unheated);  $L_{in}$ ,  $T_{in}$  = length and temperature of strand covered by blanket (heated);  $L_g$ ,  $T_g$  = length and temperature of strand embedded in girder concrete; and  $L_{bed}$  = length of casting bed (assumed unchanged by temperature change). If the strand temperature at bonding exceeds that at jacking, as is likely, the prestressing strand stress decreases (i.e.,  $\Delta f_{p1}$  is negative).

To estimate the prestressing loss for Girder 2B, the jacking temperature,  $T_j$ , was taken as 4.7°C (40.4°F), and  $T_{out}$  was taken as the ambient air temperature during curing, ranging from 0.5 to 8.4°C (33 to 47°F) (Fig. 2). Then  $T_{in}$  was taken equal to  $T_g$ , which was obtained by averaging the readings from midspan gauges BL and BR. The relevant lengths were  $L_g$  = 41.8 m (137 ft),  $L_{in}$  = 4.0 m (13 ft), and  $L_{out}$  = 15.2 m (50 ft). The resulting stress change,  $\Delta f_{p1}$ , was computed with Eq. (2) and is plotted in Fig. 3(a) as a function of bonding time. The bonding of the concrete to the steel is a gradual process, but it is likely to have started after hydration began (at 6 to 7 h) and finished before the peak temperature was reached (approximately 10 h). Applying these bounds to the data in Fig. 3(a) leads to a predicted stress change between -46.6 and -81.7 MPa (-6.8 and -11.8 ksi).

The effect that this stress loss has on the camber at release of a girder with harped strands can be calculated as

$$\Delta \delta = \frac{\Delta f_p A_p L_g^2}{8 E_{ci} I} \left[ e_{mid} + (e_{end} - e_{mid}) \frac{4 a^2}{3 L_g^2} \right] \quad (3)$$

where  $\Delta \delta$  = change in midspan camber due to change in strand stress,  $\Delta f_p$ ;  $E_{ci}$  = concrete modulus of elasticity at release;  $I$  = moment of inertia of girder;  $A_p$  = cross-sectional area of prestressing strand;  $e_{mid}$ ,  $e_{end}$  = eccentricities of prestressing strand at girder midspan and end; and  $a$  = distance from end of girder to harping point. If the bonding occurred between 6 and 10 h after casting, the change in the camber would lie between -5.7 and -10.0 mm (-0.2 and -0.4 in.) [Fig. 3(b)].

## Effects of Differing Coefficients of Thermal Expansion

If the coefficients of thermal expansion of the concrete and steel differ, the strands undergo a further stress change,  $\Delta f_{p2}$ , as the

concrete cools. This change can be calculated by applying the equations from the appendix. In the special case of a concentrically prestressed member and a spatially uniform temperature distribution, the change in stress is

$$\Delta f_{p2} = \frac{E_p}{(1 + n \rho_g)} (T_g - T_f) (\alpha_c - \alpha_p) \quad (4)$$

where  $n$  = modular ratio;  $E_p/E_c$ ,  $\rho_g$  = area of strand divided by area of concrete; and  $T_f$  = final temperature.

The effect of  $\Delta f_{p2}$  on the camber for Girder 2B was evaluated using Eqs. (3) and (4). The values of  $E_c$  (32.2 GPa, or 4,670 ksi) and  $\alpha_c$  (10.1  $\mu\epsilon/^\circ\text{C}$ , or 5.64  $\mu\epsilon/^\circ\text{F}$ ) were obtained from material samples taken at the time of casting (Barr et al. 2000b). The values for  $E_p$  (197 GPa or 28,500 ksi) and  $\alpha_p$  (12.2  $\mu\epsilon/^\circ\text{C}$  or 6.67  $\mu\epsilon/^\circ\text{F}$ ) were taken as the manufacturer-provided values. The integrals in Eqs. (10) and (11) were evaluated numerically by dividing the cross section into five regions (each surrounding a gauge) and assuming that the temperature in each region was constant. Assuming that the concrete bonds between 6 and 10 h after casting and that 20°C (68°F) is a representative service temperature, the resulting calculated stress change ranges from -5.6 to -11.6 MPa (-0.8 to -1.7 ksi.), and the corresponding camber change ranged from 4.7 to 7.8 mm (0.2 to 0.3 in.).

## Effects of Temperature Gradient at Hardening of Concrete

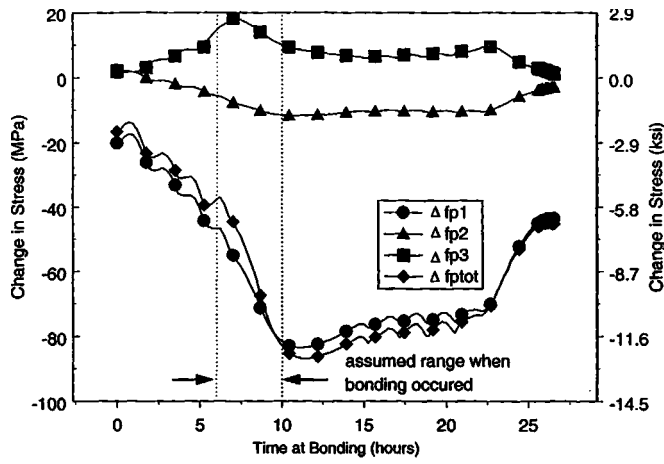
If a thermal gradient is present when the concrete hardens, thermal and mechanical strains are introduced into the cross section. When the concrete eventually cools to a uniform temperature, a change in temperature gradient will occur that is equal and opposite to the gradient induced when the concrete hardened. Specifically, if the temperature is higher at the top of the girder, as was the case in the monitored bridge girders, cooling to a uniform temperature will reduce the upward camber.

Using Eqs. (8)–(11) and assuming that the concrete hardened between 6 and 10 h after casting, the change in prestress attributable to this effect was in the range of 14.1 to 10.1 MPa (2.0 to 1.5 ksi), and the camber change was in the range of -25.1 to -37.8 mm (-1.0 to -1.5 in.).

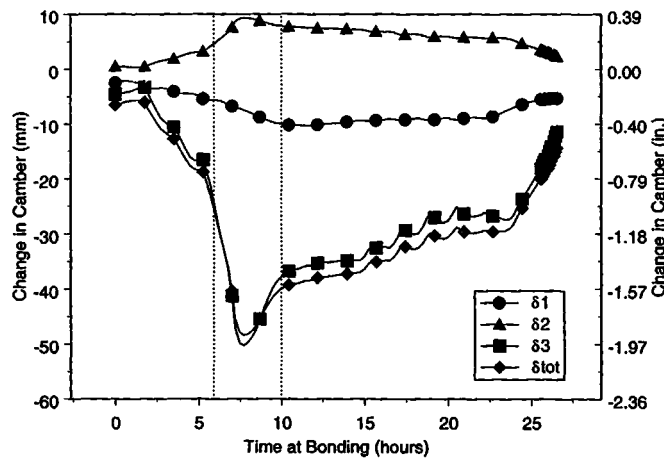
## Total Effects of High Fabrication Temperatures

Fig. 3 shows the total estimated prestress loss and change in camber, calculated as the sum of the three thermal components, as a function of the time of concrete bonding. The effects of temperature gradients ( $\Delta f_{p3}$ ,  $\delta_3$ ) tend to counteract the effects of differing coefficients of thermal expansion ( $\Delta f_{p2}$ ,  $\delta_2$ ). If the concrete bonded to the steel in the range of 6 to 10 h after casting and then cooled to the representative service temperature, the predicted change in prestress lies between -38.1 and -83.1 MPa (-5.5 and -12.1 ksi), which corresponds to 3 to 7% of the prestress at release calculated without considering thermal effects. The corresponding thermal camber changes are -26 mm (-1.0 in.) and -40 mm (-1.6 in.) for bonding times of 6 and 10 h, respectively. These values correspond to 26 and 40% of the calculated initial camber without thermal effects (99 mm).

The accuracy of these estimates can be evaluated by comparing the calculated and measured magnitudes of the camber at destressing. If thermal effects are ignored, the camber prediction (based on measured material properties) is 99 mm (3.9 in.). The predicted camber, including thermal effects, then lies between 73



(a)



(b)

**Fig. 3.** Effect of curing temperatures on Girder 2B: (a) Strand stress; and (b) camber

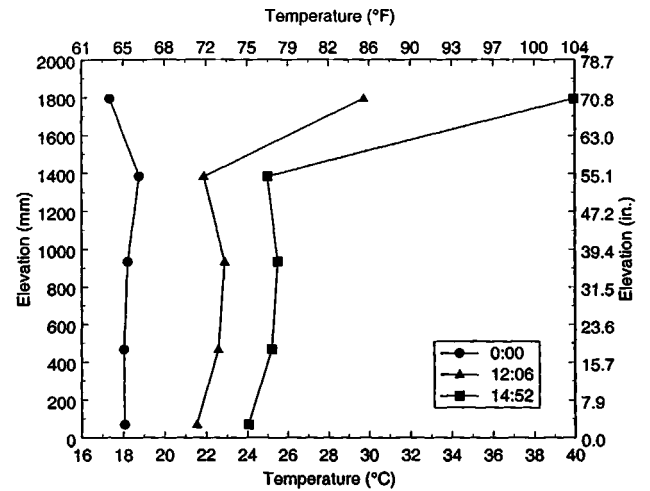
mm (2.9 in.) and 59 mm (2.3 in.). In comparison, both the stretched-wire system and the survey measurements indicated that the camber at release was 68 mm (2.7 in.).

### Effects of Variations in Service Temperature

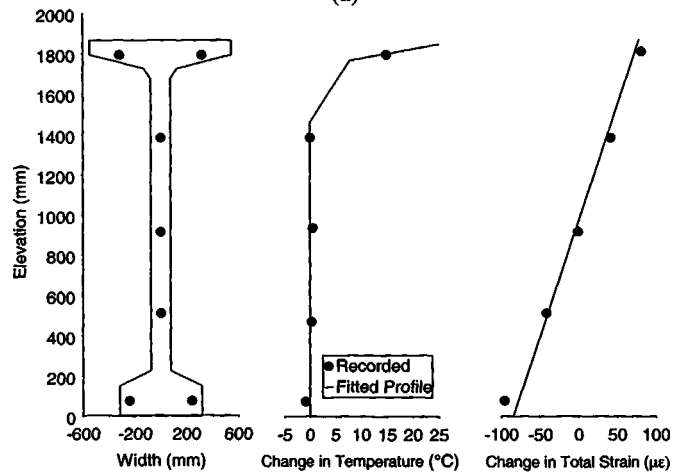
To estimate the effects of variations in service temperatures, it is necessary to select a representative temperature distribution and to calculate from it the resulting deformations and stresses. The temperature distribution in the concrete depends on the interaction of solar radiation and re-radiation, and of heat conduction and convection (Priestley 1978; Moorty and Roeder 1992). In lieu of detailed analyses of such behavior, the AASHTO (1998) specifications provide four standard design temperature profiles, which were based on a comprehensive National Cooperative Highway Research Program (NCHRP) study by Imbsen et al. (1985). The selection of the appropriate profile depends on the zone in which the bridge is located.

### Verification of Algorithm for Computing Strains

Strain and temperature readings were monitored intermittently in the test girder for 3 years from the time of casting (Barr et al. 2000a). The test girder was stored outside the Structural Engi-



(a)



(b)

**Fig. 4.** Test girder readings on June 3, 2000: (a) Temperature; and (b) strain

neering Research Laboratory at the University of Washington, allowing experimental conditions to be closely monitored. A tarp was loosely hung over each side of the girder so that only the top flange was subjected to direct sunlight. The girder rested on elastomeric bearings, permitting the girder to be modeled adequately as simply supported with no horizontal restraint.

Fig. 4(a) shows the temperatures in the test girder recorded at three times on June 3, 2000. At midnight (0.00 h), the girder concrete was coolest and the temperature distribution was nearly uniform. As the day progressed, the temperatures in the concrete increased and the distribution became significantly nonuniform. At approximately 3:00 p.m., the hottest temperature of the day was recorded, at which time the top flange (average of gauges TL and TR) was 16°C (28.8°F) hotter than the web (average of web gauges). Because the top gauges were embedded 73 mm (2.8 in.) below the top surface of the girder, the top surface concrete must have experienced an even larger increase in temperature.

To verify the relationship between temperature profile and induced strains, it is convenient to use a member, such as the test girder, in which the external forces are known accurately. Fig. 4(b) compares the measured and predicted changes in strain gradient for the test girder. The measured values represent the difference between the strains at 0.00 and 14.52 h, and the predicted values were computed from a temperature profile with the shape

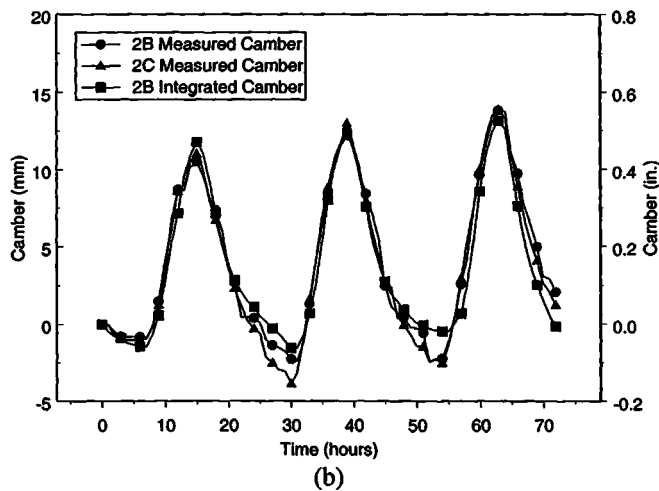
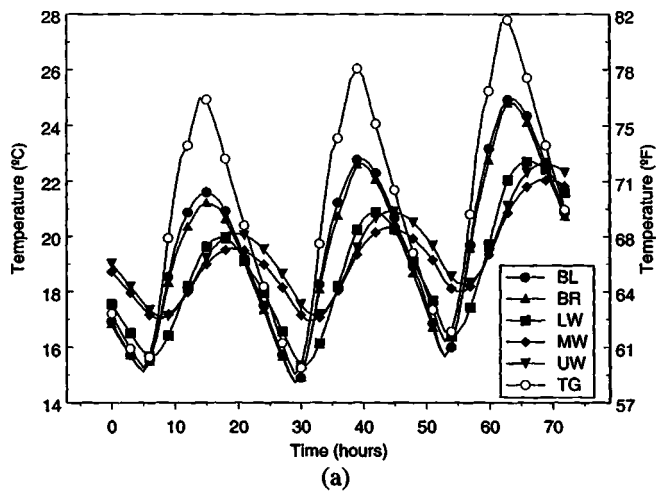


Fig. 5. Typical daily variations in Girder 2B: (a) Temperature; and (b) camber

of the AASHTO profiles and a magnitude obtained by fitting to the measured temperatures. It was necessary to adopt a standard profile shape because the sensor array was too sparse to provide a unique temperature profile. The linearity of the measured strain profile suggests that the readings are reliable. The good agreement between the predicted and measured strain gradients provides confidence in the methodology presented in the appendix.

#### Verification of Algorithm for Computing Thermal Camber

Verification of the procedure for computing camber requires a long member in which the camber change can be measured reliably. The precise end conditions for the girder do not have to be known, provided that the strain at one location is known, the end conditions are symmetric, and the thermal curvature may be assumed to be constant along the length of the bridge. The SR18/SR516 Bridge girders satisfied these conditions. Fig. 5(a) shows the temperature histories at midspan of Girder 2B for a period of 3 days (September 4 to 6, 1997). At the time, the deck had not been cast, so the top flange was exposed to direct sunlight and experienced large daily variations in temperature (gauge TG). The bottom flange (gauges BL and BR) experienced heat from the roadway below, but the web (gauges LW, MW, and UW) was partially insulated by the timber decks above and below it, so its

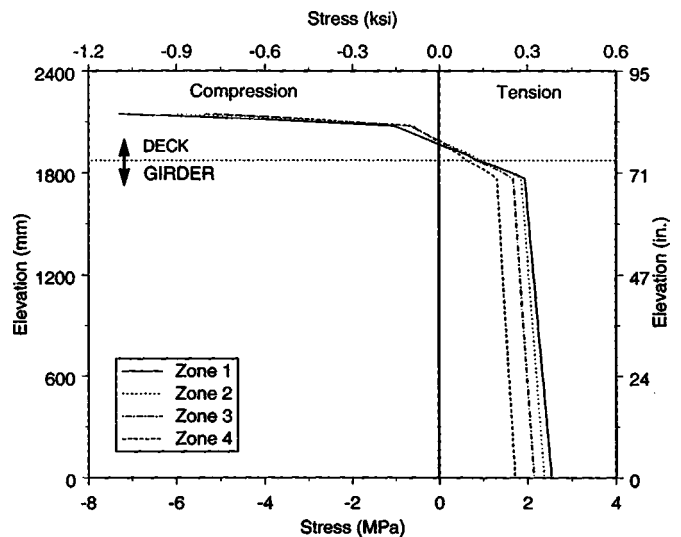


Fig. 6. Computed profiles of thermally induced stresses

temperature varied the least. The timber deck below the web was installed to prevent any construction materials from falling on the vehicles below.

Fig. 5(b) compares measured and predicted cambers for girders 2B and 2C for the 3-day period. The measured values were obtained from the automated stretched-wire systems (Stanton et al. 2003). The predicted values were obtained from integrating the curvature calculated from the measured strains, using Eq. (12).

Fig. 5(b) shows that the camber varied during the day by 15 to 20 mm (0.6 to 0.8 in.). These changes in deflection are significant; they are approximately equal to two-thirds of the deflection caused by casting the deck. The relative smoothness of the measured curves and the fact that the values for the two instrumented girders are nearly identical suggest that the measurements were reliable. The predicted and measured values are very close, which suggests that the proposed analytical procedures are accurate.

#### Stresses and Cambers Induced by AASHTO Temperature Profiles

The stresses caused by standard temperature profiles were calculated for the finished bridge. A load test performed on the bridge after completion showed that the girders behaved continuously (Barr et al. 2001). Therefore, the thermally induced stresses consisted of one component caused by the nonlinear temperature profile acting over the cross section and a second component due to the secondary moments. Fig. 6 shows the predicted design stress profiles for the SR18/SR516 girders, corresponding to the AASHTO temperature profiles for Zone 1. In this figure, tensile stress is positive and the temperature rise in the bottom flange is excluded, as it would be in most design situations. The general pattern of stresses is dominated by the secondary moments and consists approximately of compression stress in the deck and tensile stress in the girder. The Zone 1 extreme stresses were  $-8.8$  MPa ( $-1,280$  psi) at the top and  $2.5$  MPa (370 psi) at the bottom. This increase in bottom tension stress corresponds to 60% of the allowable tensile stress of  $0.5\sqrt{f'_c}$  (MPa) or  $6\sqrt{f'_c}$  (psi) and is therefore significant for design.

## Design Implications

Table 1 summarizes the changes in behavior and the consequences for design caused by accounting for the effects of thermal variations in the design. The values in the table for curing effects were calculated based on the assumption that the concrete bonded to the prestressing steel 10 h after casting. The left side of the table addresses changes in girder behavior, while the right side shows the design changes required to ensure that the girders still satisfy the AASHTO design specifications, even when thermal effects are included. To obtain the required change in the design parameter, the relevant thermal effect was included and then the girder was redesigned so that all stress limits were again satisfied. During this process, the prestress losses were reevaluated using the AASHTO refined method. The strand stress is never critical after the initial stressing, so the following discussion focuses on changes in concrete stress and camber. The values given are for the SR18/SR516 girders, but the trends are expected to be similar in other bridges.

### Consequences of Elevated Curing Temperatures

Table 1 shows that heating the strand before it bonds (Curing Effect 1) increased the bottom flange tension stress at service by up to 26% because some of the initial prestress was lost. This loss, which would be expected to occur in all prestressing plants, can be compensated for by adding tendons, if space permits. The effects of different coefficients of expansion (Effect 2) and presence of a thermal gradient (Effect 3) are much smaller. Their combined effects (Table 1) cause only a modest change in concrete stress, and this is sensitive to the shape of the thermal gradient. However, the thermal curing gradient (Effect 3) for the SR18/SR516 girders significantly reduced the camber (38%).

The effects of elevated curing temperatures on prestress loss can be compensated for by adding 12% additional prestressing reinforcement and increasing the initial concrete strength by 5%.

### Consequences of Variations in Service Temperature

The effects of in-service temperature variations differ strikingly, depending on whether the spans are continuous or simply supported. A positive temperature gradient causes compression in the bottom flange in a simply supported bridge and tension in a continuous one. However, the AASHTO (1998) specifications require that a simply supported girder also be evaluated with a negative temperature gradient equal to  $-0.3$  times the positive temperature gradient. As a result, the temperature gradient results in increased tension in the bottom flange, regardless of the support conditions.

Values based on the most severe temperature gradient (AASHTO Zone 1) are given in Table 1 for each support condition. Values for Zone 4 are about two-thirds the Zone 1 values. At midspan of the SR18/SR516 center span (Span 2), under simply supported conditions, the in-service bottom concrete tension increases by 0.42 MPa (10%). However, if the bridge is continuous, the effects of the secondary moments must be added and the net result is a 61% increase in bottom tension. Again, this excess tension can be counteracted by adding strands. However, doing so raises the initial prestress force, which in turn increases creep and prestress losses, so the required increase in the concrete strength at release (21%) is larger than the required increase in the strand area (14%).

Given the difficulties experienced in achieving the required strength of 52 MPa (7.4 ksi) in 18 h, such an increase would

likely have caused fabrication delays. One way to obtain a higher  $f'_{ci}$  quickly would be to cure at a higher temperature, but that choice is likely to lead to larger prestress losses and lower long-term concrete strength, both of which are counterproductive. Initial concrete strength is therefore an important limitation in highly stressed girders.

Continuity of the girders induces opposing changes in live load and temperature stress. By making the spans continuous, the bottom tension stress due to live load will drop while that due to in-service temperature change will rise. The magnitudes of the changes will depend on the bridge properties, but these results show that the benefits of continuity, in terms of working stresses, will diminish when thermal effects are included in the design.

### Consequences of Exceeding Stress Limits

Imbsen et al. (1985) has pointed out that neglecting thermally induced stresses has seldom led to damage in the past. Several explanations are plausible. First, the allowable tension stress of  $0.5\sqrt{f'_c}$  (MPa) is less than the true cracking stress, thereby affording some inherent safety. Second, the live-load distribution factors and other provisions in the AASHTO (1998) specifications are, on average, conservative. A third reason is that violation of the service allowable stress limits is likely to lead, at worst, to temporary cracking only under full live load. Because this behavior can be expected to occur infrequently, it is most unlikely to be noticed. The cracks will close as soon as the load is removed, so the cracking is unlikely to affect the long-term durability of the member.

The foregoing arguments illustrate that the stresses calculated with Eqs. (1a)–(1d) are nominal ones that do not reflect the in situ stresses well. Therefore, increases in the accuracy of some aspects of the model (e.g., time-stepping models of prestress loss, improved live-load distribution factors), should not necessarily be accompanied by reductions in factors of safety, particularly if other effects, such as temperature variations, are not considered.

## Conclusions

Temperatures, strains, and cambers were measured in five girders in a prestressed concrete bridge and a matching test girder. These measurements were recorded during fabrication and for 3 years while the bridge was in service. The measurements were used to study stress and camber changes caused by elevated curing temperatures and by variations in service temperatures. A method was developed for predicting the resulting variations in strains, stresses, and cambers. The accuracy of this method was then evaluated using field measurements of strain and camber.

The study led to the following conclusions:

- High curing temperatures affect both the level of prestress and the camber in a precast, prestressed concrete girder. The magnitude of this effect depends on the coefficient of thermal expansion of the materials, the temperature history during curing, its variation over the height of the girder, and the time at which the concrete bonds to the strands. For the girders monitored during this study, the strand stress was estimated to have dropped by as much as 83 MPa (12.1 ksi), which is approximately six times the computed relaxation loss. The corresponding reduction in computed camber was 40 mm (1.6 in.), which corresponds to 40% of the camber otherwise expected at distressing.
- The thermal analysis procedure described in the Appendix ac-

curately predicted the relationships between daily changes in temperature and strain and between strain and camber.

- The inclusion in design calculations of the AASHTO in-service temperature gradient significantly increases the predicted service bottom tensile stress in the girder.
- If the code working stress limits are to be satisfied, the temperature effects experienced during both curing and in service increase the prestress needed in the girders. In a highly stressed girder, an increase in required prestress will increase the losses due to elastic shortening and creep, resulting in the need for even more prestress. The demand for longer spans, and the concomitant need for higher curing temperatures to achieve higher release strengths, exacerbate this effect.
- The large number of bridge girders that are performing well in service suggests that current design procedures, in which thermal effects are often ignored, have been successful. It is likely that neglect of thermal effects has been counterbalanced by conservatism in other components of the nominal, working-stress design procedure. Therefore, proposals for reductions in conservatism should only be implemented after considering significant sources of stress, such as temperature, that are presently neglected.

## Acknowledgments

The Washington Department of Transportation and the Federal Highway Administration supported the field monitoring as part of a study of high-performance concrete in prestressed concrete girders. For their assistance throughout this project, the writers would like to thank Myint Lwin, Jerry Weigel, Bijan Khaleghi, Jen-Chi Hseih, Tom Roper, Ray Shafer (WSDOT), and Barry Brecto (FHWA). Thanks are also due to Liz Fekete, Sveinn Bjornsson, and Tom Hudgings, former graduate students at the University of Washington, for their help with the field investigation.

## Appendix. Calculation of Thermally-Induced Deformations and Stresses

Equations for calculating thermally induced stresses have been derived by several agencies [e.g., AASHTO (1989)] and researchers [e.g., Imbsen et al. (1985); Shushkewich (1998)]. General equations, which account for the presence of several materials in the cross section, such as precast concrete, cast-in-place concrete, prestressing strand, and deformed bar steel, are derived here. Stresses and deformations induced by differential shrinkage of the various components can also be computed using the same equations if the free shrinkage strain is used in place of the free thermal strain and an age-adjusted effective modulus is used for the concrete. The equations are used in the paper to determine the effects of thermal loading.

### Externally Determinate Girders

Fig. 7(a) shows a typical bridge girder in service. Heating the top of the bridge deck, as typically occurs during the day, causes the free thermal strains shown in Fig. 7(b), which are calculated using Eq. (5).

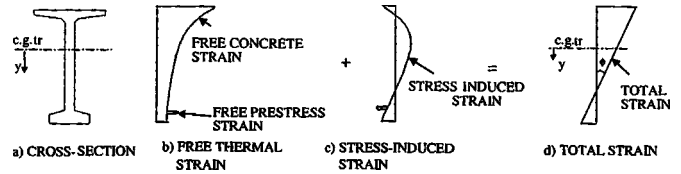


Fig. 7. Strain distribution in simply supported girder

$$\varepsilon_{th}(y) = \alpha_i \Delta T(y) \quad (5)$$

where  $\varepsilon_{th}(y)$  = free thermal strain at any height,  $y$ , in the cross section,  $y$  = vertical coordinate measured downward from composite centroid;  $\alpha_i$  = coefficient of thermal expansion of material  $i$ ; and  $\Delta T(y)$  = temperature change at height  $y$  relative to temperature at construction.

The total strain field is assumed to be linear [Fig. 7(d)] in accordance with the Bernoulli hypothesis, so mechanical (i.e., stress-induced) strains, shown in Fig. 7(c), will be introduced. The total strain is then

$$\varepsilon_{tot}(y) = \varepsilon_{th}(y) + \varepsilon_{mech}(y) \quad (6)$$

where  $\varepsilon_{tot}(y)$  is the total strain and  $\varepsilon_{mech}(y)$  is the mechanical strain. The total linear strain field can be described by

$$\varepsilon_{tot}(y) = \varepsilon_0 + y\phi_0 \quad (7)$$

where  $\varepsilon_0$  is the strain at the centroid of the cross section and  $\phi_0$  is the curvature. Positive curvature is defined in the same sense as is positive moment. The stress at height  $y$  in material  $i$  is obtained from Eqs. (5) and (6) as

$$\sigma_i(y) = E_i \varepsilon_{mech}(y) = E_i [\varepsilon_{tot}(y) - \alpha_i \Delta T(y)] \quad (8)$$

Axial force equilibrium requires

$$0 = \int \sigma dA = \sum_i E_i \int [\varepsilon_{tot}(y) - \alpha_i \Delta T(y)] dA_i \quad (9)$$

Substituting for  $\varepsilon_{tot}$  in Eq. (9) leads to the centroidal strain

$$\varepsilon_0 = \frac{\sum_i \alpha_i E_i \int \Delta T(y) dA_i}{\sum_i E_i A_i} \quad (10)$$

Similar logic for moment equilibrium leads to the following strain gradient or curvature:

$$\phi_0 = \frac{\sum_i \alpha_i E_i \int \Delta T(y) y dA_i}{\sum_i E_i I_i} \quad (11)$$

If the temperature profile is known, the variables  $\varepsilon_0$  and  $\phi_0$ , which fully define the strain field, can be computed with Eqs. (10) and (11). The resulting stress induced at any level can then be computed with Eq. (8). The integrals in Eqs. (10) and (11) can easily be evaluated numerically.

Camber can be obtained by integrating the curvatures. For example, if the curvature is uniform over a simple span, the mid-span camber is given by

$$\delta = \frac{\phi_0 L^2}{8} \quad (12)$$

These equations allow for a variety of materials in the cross section, and their derivation does not require the addition and subsequent removal of the restraint moments and forces typically used by others [e.g., Imbsen et al. (1985); Shushkewich (1998)]. The format of Eqs. (10) and (11) allows all responses to be computed directly. For example, if the properties of the concrete in the girder and deck differ, Eq. (11) directly predicts a camber change even for a uniform temperature profile. Obtaining this result is more complex if the calculations are conducted in terms of forces.

### Externally Indeterminate Girders

In a continuous girder, the tendency to camber is restrained by the supports. These restraint forces lead to secondary moments over the supports (Imbsen et al. 1985). Therefore, for a continuous girder, the temperature-induced stresses are the sum of the statically determinate thermally induced stresses and the stresses produced by the secondary moments.

### References

- American Concrete Institute (ACI). (1999). *Building code requirements for structural concrete and commentary*, Committee 318, Farmington Hills, Mich.
- Acker, P., and Hassan, M. (1978). "Prestress loss of thermal origin during production of pretensioned concrete elements." *Rep. LPC No. 78*, Laboratoire Central des Ponts et Chaussées, Paris (in French).
- American Association of State Highway and Transportation Officials (AASHTO). (1989). *AASHTO guide specifications thermal effect in concrete bridge superstructures*, Washington, D.C.
- American Association of State Highway and Transportation Officials (AASHTO). (1996). *Standard specifications for highway bridges*, 16th Ed., Washington, D.C.
- American Association of State Highway and Transportation Officials (AASHTO). (1998). *LRFD bridge design specifications*, 2nd Ed., Washington, D.C.
- Barr, P. J. (1998). "Behavior of high performance prestressed concrete girders." MSCE thesis, Univ. of Washington, Seattle.
- Barr, P. J., Eberhard, M. O., and Stanton, J. F. (2001). "Live-load distribution factors for prestressed concrete girder bridges." *J. Bridge Eng.*, 6(5), 298–306.
- Barr, P. J., Eberhard, M. O., Stanton, J. F., Khaleghi, B., and Hsieh, J. C. (2000a). "High performance concrete in Washington State SR18/SR516 overcrossing." *Final Rep. on Girder Monitoring*, Washington State Dept. of Transportation, Olympia, Wash.
- Barr, P. J., Fekete, E., Stanton, J. F., and Eberhard, M. O. (2000b). "High performance concrete in Washington State SR18/SR516 overcrossing." *Final Rep. on Materials Tests*, Washington State Dept. of Transportation, Olympia, Wash.
- Burns, N. H., Gross, S. P., and Byle, K. A. (1997). "Instrumentation and measurements—Behavior of long-span prestressed high performance concrete bridges." *Proc., PCI/FHWA Int. Symp. on High Performance Concrete*, Ottawa, 566–577.
- Ghali, A., and Elbadry, M. (1997). "Monitoring of deflections of the Confederation Bridge, Canada." *Proc., Annual Conf. of the Canadian Society for Civil Engineering*, Montreal, 161–166.
- Lwin, M. M., and Khaleghi, B. (1997). "Time-dependent prestress losses in prestress girders built of high performance concrete." *Transportation Research Record*, 76th Annual Meeting, Transportation Research Board, Washington, D.C., 64–72.
- Huang, T. (1982). "Study of prestress losses conducted by Lehigh University." *PCI J.*, 27(5), 48–61.
- Imbsen, R. A., Vandershaf, D. E., Schamber, R. A., and Nutt, R. V. (1985). "Thermal effects in concrete bridge superstructures." *NCHRP Proj. Rep. 12-22*, Transportation Research Board, Washington, D.C.
- Ma, Z., Huo, X., Tadros, M. K., and Baishya, M. (1998). "Restraint moments in precast/prestressed concrete continuous bridges." *PCI J.*, 43(6), 40–57.
- Mehta, P. K., and Monteiro, P. J. (1993). *Concrete: Structure, properties and materials*, Prentice-Hall, Englewood Cliffs, N.J.
- Moorthy, S., and Roeder, C. W. (1992). "Temperature dependent bridge movements." *J. Struct. Eng.*, 118(4), 1090–1105.
- Priestley, M. J. N. (1978). "Design of concrete bridges for temperature gradients." *ACI J.*, 75(5), 209–217.
- Seguirant, S. J. (1998). "New deep sections extend spans of prestressed concrete girders." *PCI J.*, 43(4), 92–119.
- Shushkewich, K. W. (1998). "Design of segmental bridge for thermal gradient." *PCI J.*, 43(4), 120–137.
- Stanton, J. F., Eberhard, M. O., and Barr, P. J. (2002). "A weighted stretched-wire system for monitoring deflections." *Structural and Geotechnical Engineering and Mechanics Rep. SGEM 02-01*, Univ. of Washington, Seattle.
- Stanton, J. F., Eberhard, M. O., and Barr, P. (2003). "A weighted-stretched-wire system for monitoring deflections." *Eng. Struct.*, 25, 347–357.
- Vurpillot, S., Kruefer, G., Benouaich, D., Clement, D., and Inaudi, D. (1998). "Vertical deflection of a prestressed concrete bridge using deformation sensors and inclinometer measurements." *ACI Struct. J.*, 95(5), 518–526.